International Journal of Engineering Research and Advanced Technology (IJERAT)

DOI: 10.31695/IJERAT.2021.3721

E-ISSN : 2454-6135

Volume.7, No. 8
August -2021

Higher Order Semi- Analytical Method: Analysis of Up & Down - Milling Stability of High Speed Machining

Mohamadou Balarabé[1], Beda Tibi[1], Nzié Wolfgang[2] & Pehma Elkana[3]

[1] Department of Physics, Faculty of Sciences,
University of Ngaoundéré,
PO.BOX 454 Ngaoundéré, Cameroon
[2] Department of Mechanics, University Institute of Technology,
University of Ngaoundéré, PO.BOX 454 Ngaoundéré, Cameroon
[3] Department of Physics, Faculty of Sciences, University of Yaoundé,
PO.BOX 337 Yaoundé, Cameroon

ABSTRACT

This work presents dynamic stability analysis of general high speed milling process by higher order semi-analytical method. The first order full-discretization method (1st FDM) and second order full-discretization method (2nd FDM) are presented. These methods based on the direct integration scheme. The governing mathematical model applied is the delay- differential equation with single time periodic delay taking regenerative effect into account. The stability lobes diagrams are presented for single degree of freedom mechanical model and two degree of freedom mechanical model. Up- milling and down-milling stability chart are presented for various radial immersion ratio in order to compare accuracy of up- and down-milling. It is demonstrated that for full-immersion down- milling and up- milling stability lobes diagram are the same approximatively but in other cases down-milling is more accuracy than up-milling both for single degree of freedom and two degree of freedom.the computational time of calculation of eigenvalue is also variable for different computational parameter. The rate of convergence for half immersion and low immersion is presented for variable parameters.

Key Words*:* High Speed Machining, Milling Stability, Chatter, Semi-Analytical Method**.**

1 INTRODUCTION

High Speed Machining (HSM) enables the possibility not only to reduce process time but other and above all to improve workpiece accuracy and workpiece surface. HSM is mostly related to the application of high cutting speeds higher than in conventional machining. Althout his importance to resolve many lacks of tradditional machining and economical fact, HSM has a serious problem that made us a lot of attention. One of the most intriguing problems that face HSM process is self-excited vibrations known in the literature as chatter. Regenerative chatter and mode coupling chatter was followed as the mains sources of self-excited vibration by authors [1] and [2]. Zhang, et al. investigated the occurrence of both chatters using different cutting tools [3]. During their experiments, the regenerative chatter was observed while using a long flexible tool and mode coupling chatter was observed while using a short tool with larger stuffiness. The authors explained that the different results are due to the impact of tool structure which changes the stability boundary for both chatter mechanisms. The regenerative chatter occurs when the subsequent machining on the rough surface after the previous cutting path. During milling, the next tooth in cut collides with the wavy surface of the previous tooth and generates a new wavy surface. The chip thickness and the cutting force vary due to the phase difference between the wave left by the previous tooth and the wave generated by the current one [4]. On the other hand, mode coupling chatter means the vibration exists simultaneously in two or more directions coupling to each other with different characteristics. Tlusty and Ismail explained that mode coupling effect may occur if the natural modes are closely matched in principal directions[5]. Without any regeneration, the structure vibrates simultaneously in the different directions at the same frequency and a phase shift.

Generally, the dynamic of the milling is modeled by delayed differential equations (DDEs) with time periodic parameters. For chatter stability in milling process stability lobes diagram is necessary to predict optimal selection of spindle speed and cutting depth to prevent chatter and to ameliorate production efficiency. Many methods have been put forward to predict chatter stability in milling process. Zero order frequency method was presented by Altintas and Budak, they used the Fourier series expansions for periodic terms but only the constant term in each Fourier series expansion is considered [6]. In order to ameliorate the application

of the frequency domain methods, Budak and Altintas presented also the multi-frequencies method [7]. The multi-frequencies method is expand by [8]. The stability analysis is performed by expanding the periodic matrix into Fourier series, and using the basic physical properties of dynamic cutting and regeneration mechanism. Ding *et al* proposed an efficient and accurate time domain method through directly approximating the original Delay Differential Equation by algebraic equations based on the differential quadrature method (DQM), without the help of the integral equation [9]. Butcher and co-workers presented the Chebyshev polynomial based method, the stability charts are produced for several examples of time-periodic DDEs, including the delayed Mathieu equation and a model for regenerative chatter in impedance-modulated turning and the Chebyshev collocation method [10,11]. They used a collocation expansion of the solution at the Chebyshev collocation points during the cutting period, and a state transition matrix for the free-vibration period where no cutting occurs.

Several author presented semi- discretization method (SDM) for milling stability analysis. SDM was applied to determine the stability charts of the Mathieu equation for delayed systems by [12]. Elbeyli and co-worker presented and analyzed Zeroth-, improved zeroth- and first-order versions of the SDM technique for a second order periodic system with time delay for feedback control design of linear systems with time delay [13]. Insperger *et al* extended to the higher order SDM [14]. They introduced this method to determine the stability charts of the Mathieu equation with continuous time delay. Updated semi-discretization method for periodic delay- differential equations with discrete delay was presented by Insperger and coworker [15]. They established the convergence of the semi-discretization approximation method for a class of delay equations modeling the milling process and they showed that semi-discretization preserves asymptotic stability of the original equation, thus it can be used to obtain good approximations for the stability charts. Henninger *et al* presented an improved the computational efficiency and accuracy of the semi- discretization method for periodic delay-differential equations. The improving SDM increased computational efficiency of the semi-discretization method [16]. Ahmadi and Ismail in 2012 presented Multi-Frequency Solution and the Semi-Discretization Method to establish the stability lobes in milling by using damping process [17]. The basic formulations are presented along with the comparisons between the two approaches. It is shown that the Semi-Discretization Method provides accurate results over the whole tested range of cutting speed, whereas higher harmonics are required to achieve the same accuracy when applying the Multi-Frequency Solution at low speeds. Wang et al. studied the regenerative chatter in the high-speed vertical milling of thin-walled workpiece made of titanium alloy based on the frequency domain method [18].

In the last decade Ding *et al* [19] proposed firstly the full- discretization method based on the direct integration scheme. They presented stability lobes by varying the radial immersion ratio only. Second order full- discretization method based on the direct integration scheme are presented by them but the stability lobes are presented in the case of different computational parameter [20]. The third order full-discretization was studied by [21,22] point of these methods is that the dynamics of the milling process considering the regenerative effect is described by a linear time periodic system with a single discrete time delay, and the response of the system is calculated by a direct integration scheme with the help of discretizing the time period. Higher order FDM was presented by Ozoegwu in 2015 presented four and five order cases full- discretization method in order for the first time settle this curiosity of what becomes of accuracy of the full-discretization method beyond third order theory [23]. They are increase of convergence but decrease of computational time. Insperger presented Full- discretization and semi-discretization for milling stability prediction [24]. It was shown that the FDM and the SDM are similar in the sense that both methods approximates the original Delay Differntial Equation by a series of Ordinary Differential Equations(ODEs). Recently Zhang proposed Simpson method to resolve charter stability problem and his result is very simple than higher order semi discretization [25]. Jin Bo and co-workers introduced a generalized form of the Runge–Kutta method (GRKM) based on the Volterra integral equation of the second kind. It was shown that the method had higher convergence rate and computation accuracy, validated by comparisons with the semi- discretization method [26]. More recently the so-called semi-analytical holistic interpolation method (HIM) with both high efficiency and accuracy was proposed by Cheng jin and co-worker to predict stability of milling processes which reduce more computational time than Update Full Discretization Method (UFDM) [27].

Several author introduced two main analytical methods for stability prediction of general milling operation, the finite element analysis in time method (FEATM) and the SDM. They presented up- milling and down- milling stability analysis for varying radial immersion for single degree of freedom and single fluted tool [28,29]. The aim of this research is to make the comparison of stability lobes diagram in order to enlarge study and increase stability in high speed milling process by using 2^{nd} FDM. This work presented stability analysis of chatter stability of up- and down-milling process. This article is organized as follows: the introduction of cutting models, a model equations and stability analysis of milling process is presented in Sect. 2, Application of numerical simulation of the milling stability are offered in Sect. 3, stability diagrams in Sect. 4, rate of convergence in Sect. 5 we offer our conclusions in sect. 6.

2 MODEL EQUATIONS AND STABILITY ANALYSIS OF MILLING PROCESS

[19,25, 32] presented the dynamic milling process taking the regenerative effect into account as follow

DOI : 10.31695/IJERAT.2021.3721

$$\dot{\mathbf{u}}(t) = \boldsymbol{A}\mathbf{u}(t) + \boldsymbol{B}(t)\mathbf{u}(t) + \boldsymbol{C}(t)\mathbf{u}(t-T) \tag{1}$$

Where $\boldsymbol{A}$ is a constant matrix representing the time invariant nature of the system. $\boldsymbol{B}(t)$ and $\boldsymbol{C}(t)$ are the periodic-coefficients matrix with $\mathbf{B}(t) = \mathbf{B}(t+T)$ and $\boldsymbol{C}(t) = \boldsymbol{C}(t+T)$, T is the regenerative delay which equals to the time period and $\mathbf{u}(t)$ is the state variable of the system.

The solution of (5) can be expressed using direct integration scheme as follow

$$\boldsymbol{u}(t) = e^{(t-\alpha\tau)}\mathbf{u}(\alpha\tau) + \int_{(\alpha\tau)}^{t} \{e^{(t-\varepsilon)}[\mathbf{B}(\varepsilon)\boldsymbol{u}(\varepsilon) + \mathbf{C}(\varepsilon)\mathbf{u}(\varepsilon - T)]\}d\varepsilon \tag{2}$$

Where $\mathbf{u}((\alpha\tau+\tau)$ denote the value of $\boldsymbol{u}(t)$ at $t = (\alpha\tau+\tau)$. $\mathbf{u}(\alpha\tau+\tau)$ can be obtained from (2) as follow

$$\mathbf{u}(\alpha\tau+\tau) = e^{A\tau}\mathbf{u}(\alpha\tau) + \int_{0}^{\tau} \{e^{A\varepsilon}[\mathbf{B}(\alpha\tau+\tau-\varepsilon)\mathbf{u}(\alpha\tau+\tau-\varepsilon)]\}d\varepsilon + \int_{0}^{\tau} \{e^{A\varepsilon}\big[\mathbf{C}\big((\alpha\tau+\tau-\varepsilon)\big)\mathbf{u}(\alpha\tau+\tau-\varepsilon-T)\big]\}d\varepsilon \tag{3}$$

Equation (8) can be expressed as follows

$$\mathbf{u}\big((\alpha+1)\tau\big) = e^{A\tau}\mathbf{u}(\alpha\tau) + \int_{0}^{\tau} \{e^{A\varepsilon}[\mathbf{B}(\alpha\tau+\tau-\varepsilon)\mathbf{u}(\alpha\tau+\tau-\varepsilon)]\}d\varepsilon + \int_{0}^{\tau} \{e^{A\varepsilon}\big[\mathbf{C}\big((\alpha\tau+\tau-\varepsilon)\big)\mathbf{u}(\alpha\tau+\tau-\varepsilon-T)\big]\}d\varepsilon \tag{4}$$

$\mathbf{B}(\alpha\tau+\tau-\varepsilon)$, $\mathbf{C}(\alpha\tau+\tau-\varepsilon)$ are the time - periodic item. It is approximated by linearly the first-order Lagrange interpolation polynomial; the two boundary values at the time interval$[\alpha\tau, (\alpha\tau+\alpha)]$, resulting in

$$\mathbf{B}(\alpha\tau+\tau-\varepsilon) = B_0^{(\alpha)} + \varepsilon B_1^{(\alpha)} \tag{5}$$

$$\mathbf{C}(\alpha\tau+\tau-\varepsilon) = C_0^{(\alpha)} + \varepsilon C_1^{(\alpha)} \tag{6}$$

Where $B_0^{(\alpha)} = \mathbf{B}_{\alpha+1}$, $\mathbf{C}_0^{(\alpha)} = \mathbf{C}_{\alpha+1}$ and $B_1^{(\alpha)} = (\mathbf{B}_\alpha - \mathbf{B}_{\alpha+1})/\tau$, $C_1^{(\alpha)} = (\mathbf{C}_\alpha - \mathbf{C}_{\alpha+1})/\tau$ and $\mathbf{B}_\alpha$ and $\mathbf{C}_\alpha$ denote respectively the value of $\mathbf{B}(t)$and $\mathbf{C}(t)$ sampled at the time $\mathbf{t}_\alpha = \alpha\tau$.

2.1 First order Full-Discretization Method

For first order discretization the state item $\mathbf{u}(\alpha\tau+\tau-\varepsilon)$ and delayed term $\mathbf{u}(\alpha\tau+\tau-\varepsilon-T)$ are both in. (4) can be approximated too linearly using $\mathbf{u}_\alpha$, $\mathbf{u}_{\alpha+1}$ and$\mathbf{u}_{\alpha-m}$, $\mathbf{u}_{\alpha+1-m}$ respectively, i.e the two boundary values at the time interval$[\alpha\tau, (\alpha+1)\tau]$ and $[(\alpha-m\tau), (\alpha+1-m)\tau]$ respectively.

$$\mathbf{u}(\alpha\tau+\tau-\varepsilon) = \mathbf{u}_{\alpha+1} + \frac{\varepsilon(\mathbf{u}_\alpha - \mathbf{u}_{\alpha+1})}{\tau} \tag{7}$$

$$\mathbf{u}(\alpha\tau+\tau-\varepsilon-T) = \mathbf{u}_{\alpha+1-m} + \frac{\varepsilon(\mathbf{u}_{\alpha-m} - \mathbf{u}_{\alpha+1-m})}{\tau} \tag{8}$$

Substituting (5)- (8) into (4) leads to

$$\boldsymbol{u}_{\alpha+1} = [I - G_{\alpha+1}]^{-1}G_\alpha\mathbf{u}_\alpha - [I - G_{\alpha+1}]^{-1}G_{m-1}\mathbf{u}_{\alpha+m-1} - [I - G_{\alpha+1}]^{-1}G_m\mathbf{u}_{\alpha-m} \tag{9}$$

Where

$$G_{\alpha+1} = \left(\frac{Z_2 - Z_3}{\tau^2}\right)B_\alpha + \left(\frac{Z_1 - Z_2}{\tau} - \frac{Z_2 - Z_3}{\tau^2}\right)B_{\alpha+1} \tag{10}$$

$$G_\alpha = \left(\frac{Z_2}{\tau^2}\right)B_\alpha + \left(\frac{Z_2}{\tau} - \frac{Z_3}{\tau^2}\right)B_{\alpha+1} + Z_0 \tag{11}$$

$$G_{\alpha-1} = \left(\frac{Z_2 - Z_3}{\tau^2}\right)B_\alpha + \left(\frac{Z_1 - Z_2}{\tau} - \frac{Z_2 - Z_3}{\tau^2}\right)B_{\alpha+1} \tag{12}$$

DOI : 10.31695/IJERAT.2021.3721

$$G_m = \left(\frac{Z_3}{\tau^2}\right) B_\alpha + \left(\frac{Z_2}{\tau} - \frac{Z_3}{\tau^2}\right) B_{\alpha+1} \tag{13}$$

The matrices $Z_1 - Z_3$ in $(14) - (16)$ are presented and expressed explicitly in terms of matrices Z_0 and A^{-1} as follows:

$$Z_1 = \int_0^\tau e^{A\varepsilon}\, d\varepsilon = A^{-1}(e^{A\tau} - I) = A^{-1}(Z_0 - I) \tag{14}$$

$$Z_2 = \int_0^\tau \varepsilon e^{A\varepsilon}\, d\varepsilon = \varepsilon A^{-1} e^{A\tau} - A^{-1} \int_0^\tau e^{A\varepsilon}\, d\varepsilon = A^{-1}(Z_0 - \tau^{-1} Z_1) \tag{15}$$

$$Z_3 = \int_0^\tau \varepsilon^2 e^{A\varepsilon}\, d\varepsilon = A^{-1}(Z_0 - 2\tau^{-2} Z_2) \tag{16}$$

The matrix form of. (8) can be expressed as follow:

$$\begin{bmatrix} \boldsymbol{u}_{\alpha+1} \\ \boldsymbol{u}_{\alpha} \\ \boldsymbol{u}_{\alpha-1} \\ \boldsymbol{u}_{\alpha-2} \\ \vdots \\ \boldsymbol{u}_{\alpha+4-k} \\ \boldsymbol{u}_{\alpha+3-k} \\ \boldsymbol{u}_{\alpha+2-k} \\ \boldsymbol{u}_{\alpha+1-k} \end{bmatrix} = \begin{bmatrix} \mathbf{S}^{1,1} & 0 & 0 & 0 & \cdots & 0 & 0 & \mathbf{S}^{1,\mathrm{m}} & \mathbf{S}^{1,\mathrm{m}+1} \\ 1 & 0 & 0 & 0 & \cdots & 0 & 0 & 0 & 0 \\ 0 & 1 & 0 & 0 & \cdots & 0 & 0 & 0 & 0 \\ 0 & 0 & 1 & 0 & \cdots & 0 & 0 & 0 & 0 \\ \vdots & \vdots & \vdots & \vdots & \ddots & \vdots & \vdots & \vdots & \vdots \\ 0 & 0 & 0 & 0 & \ldots & 0 & 0 & 0 & 0 \\ 0 & 0 & 0 & 0 & \cdots & 1 & 0 & 0 & 0 \\ 0 & 0 & 0 & 0 & \cdots & 0 & 1 & 0 & 0 \\ 0 & 0 & 0 & 0 & \cdots & 0 & 0 & 1 & 0 \end{bmatrix} \begin{bmatrix} \boldsymbol{u}_{\alpha} \\ \boldsymbol{u}_{\alpha-1} \\ \boldsymbol{u}_{\alpha-2} \\ \boldsymbol{u}_{\alpha-3} \\ \vdots \\ \boldsymbol{u}_{\alpha+3-k} \\ \boldsymbol{u}_{\alpha+2-k} \\ \boldsymbol{u}_{\alpha+1-k} \\ \boldsymbol{u}_{\alpha-k} \end{bmatrix} \tag{17}$$

Where

$$\mathbf{S}^{1,1} = [I - G_{\alpha+1}]^{-1} G_\alpha \tag{18}$$

$$\mathbf{S}^{1,\mathrm{m}} = [I - G_{\alpha+1}]^{-1} G_{m-1} \tag{19}$$

$$\mathbf{S}^{1,\mathrm{m}+1} = [I - G_{\alpha+1}]^{-1} G_m \tag{20}$$

the discrete map according to eq.8 can be defined as follow

$$\boldsymbol{u}_{\alpha+1} = D_\alpha \boldsymbol{u}_\alpha \tag{21}$$

D_α is expressed as

$$D_\alpha = \begin{bmatrix} \mathbf{S}^{1,1} & 0 & 0 & 0 & \cdots & 0 & 0 & \mathbf{S}^{1,\mathrm{m}} & \mathbf{S}^{1,\mathrm{m}+1} \\ \mathrm{I} & 0 & 0 & 0 & \cdots & 0 & 0 & 0 & 0 \\ 0 & \mathrm{I} & 0 & 0 & \cdots & 0 & 0 & 0 & 0 \\ 0 & 0 & \mathrm{I} & 0 & \cdots & 0 & 0 & 0 & 0 \\ \vdots & \vdots & \vdots & \vdots & \ddots & \vdots & \vdots & \vdots & \vdots \\ 0 & 0 & 0 & 0 & \ldots & 0 & 0 & 0 & 0 \\ 0 & 0 & 0 & 0 & \cdots & \mathrm{I} & 0 & 0 & 0 \\ 0 & 0 & 0 & 0 & \cdots & 0 & \mathrm{I} & 0 & 0 \\ 0 & 0 & 0 & 0 & \cdots & 0 & 0 & \mathrm{I} & 0 \end{bmatrix} \tag{22}$$

The approximate Floquet transition matrix is obtained as:

$$\boldsymbol{y}_\alpha = \boldsymbol{D}_{\alpha-1}\boldsymbol{x}_{\alpha-1} = \boldsymbol{D}_{\alpha-1}\boldsymbol{D}_{\alpha-2}\boldsymbol{x}_{\alpha-2} = \cdots = \boldsymbol{D}_{\alpha-1}\boldsymbol{D}_{\alpha-2}\boldsymbol{D}_{\alpha-3} \ldots \boldsymbol{D}_0 \boldsymbol{x}_0 \tag{23}$$

The transition matrix Ψ is given by the simple matrix multiplication. It gives the connection between $\boldsymbol{y}_0$ and $\boldsymbol{y}_\alpha$. The transformation matrix during one period Ψ is:

DOI : 10.31695/IJERAT.2021.3721

$$\Psi = \boldsymbol{D}_{\alpha-1}\boldsymbol{D}_{\alpha-2}\boldsymbol{D}_{\alpha-3}\dots\boldsymbol{D}_3\boldsymbol{D}_1\boldsymbol{D}_0 \tag{24}$$

The stability of the system can be determined by using the eigenvalues of the transition matrix Ψ are in modulus less than unity, the system is stable, otherwise, it will be unstable

2.2 2nd Full-Discretization Method

For the second order the state item $\mathbf{u}(\alpha\tau+\tau-\varepsilon)$ in (4) can be approximated by second-degree Lagrange polynomial by using $\mathbf{u}_\alpha$,$\mathbf{u}_{\alpha-1}$and $\mathbf{u}_{\alpha+1}$ i.e the three boundary values at the time interval $[(\alpha-m)\tau,(\alpha+1-m)\tau]$,

$$\mathbf{u}(\alpha\tau+\tau-\varepsilon)=\frac{(\tau-\varepsilon)(2\tau-\varepsilon)}{2\tau^2}\mathbf{u}_{\alpha+1}+\frac{\varepsilon(2\tau-\varepsilon)}{\tau^2}\,\mathbf{u}_\alpha+\frac{\varepsilon(\varepsilon-\tau)}{2\tau^2}\mathbf{u}_{\alpha-1} \tag{25}$$

Substituting. (5),(6),(8) and (22) into (25) leads to

$$\begin{aligned}\mathbf{u}(\alpha\tau+\tau)=e^{\mathbf{A}\varepsilon}\mathbf{u}(\alpha\tau)&+\int_0^\tau e^{A\varepsilon}\left[\left[\frac{\varepsilon^2}{2\tau^2}-\frac{\varepsilon}{2\tau}\right]\mathbf{u}_{\alpha-1}+\left[\frac{2\varepsilon}{\tau}-\frac{\varepsilon^2}{\tau^2}\right]\mathbf{u}_\alpha+\left[1-\frac{3\varepsilon}{2\tau}+\frac{\varepsilon^2}{2\tau^2}\right]\mathbf{u}_{\alpha+1}\right]B_0^{(\alpha)}d\varepsilon\\&+\int_0^\tau e^{A\varepsilon}\left[\left[\frac{\varepsilon^3}{2\tau^2}-\frac{\varepsilon^2}{2\tau}\right]\mathbf{u}_{\alpha-1}+\left[\frac{2\varepsilon^2}{\tau}-\frac{\varepsilon^3}{\tau^2}\right]\mathbf{u}_\alpha+\left[\varepsilon-\frac{3\varepsilon^2}{2\tau}+\frac{\varepsilon^3}{2\tau^2}\right]\mathbf{u}_{\alpha+1}\right]B_1^{(\alpha)}d\varepsilon\\&-\int_0^\tau e^{A\varepsilon}\left[\left[1-\frac{\varepsilon}{\tau}\right]\mathbf{u}_{\alpha+1-m}+\frac{\varepsilon}{\tau}\mathbf{u}_{\alpha-m}\right]B_0^{(\alpha)}d\varepsilon-\int_0^\tau e^{A\varepsilon}\left[\left[\varepsilon-\frac{\varepsilon^2}{\tau}\right]\mathbf{u}_{\alpha+1-m}+\frac{\varepsilon^2}{\tau}\mathbf{u}_{\alpha-m}\right]B_1^{(\alpha)}d\varepsilon\end{aligned} \tag{26}$$

Equation (26) can be expressed using the following equation

$$\boldsymbol{u}_{\alpha+1}=\boldsymbol{G}_{\alpha+1}\boldsymbol{u}_{\alpha+1}+\boldsymbol{G}_\alpha\mathbf{u}_\alpha+\boldsymbol{G}_\alpha\mathbf{u}_\alpha+\boldsymbol{G}_{\alpha-1}\mathbf{u}_{\alpha-1}-\boldsymbol{G}_{m-1}\mathbf{u}_{\alpha+m-1}-G_m\mathbf{u}_{\alpha-m} \tag{27}$$

Where

$$G_{\alpha+1}=\left(\frac{Z_2}{\tau}-\frac{3Z_3}{2\tau^2}+\frac{Z_4}{2\tau^3}\right)B_\alpha+\left(\left(Z_1-\frac{3Z_2}{2\tau}+\frac{Z_3}{2\tau^2}\right)-\left(\frac{Z_2}{\tau}-\frac{3Z_3}{2\tau^2}+\frac{Z_4}{2\tau^3}\right)\right)B_{\alpha+1} \tag{28}$$

$$G_\alpha=\left(\frac{2Z_3}{2\tau^2}-\frac{Z_4}{\tau^3}\right)B_\alpha+\left(\left(\frac{2Z_2}{\tau}-\frac{Z_3}{\tau^2}\right)-\left(\frac{2Z_3}{2\tau^2}-\frac{Z_4}{\tau^3}\right)\right)B_{\alpha+1}\;+\;G_0 \tag{29}$$

$$G_{\alpha-1}=\left(\frac{Z_4}{2\tau^3}-\frac{Z_3}{2\tau^2}\right)B_\alpha+\left(\left(\frac{Z_3}{2\tau^2}-\frac{Z_2}{2\tau}\right)-\left(\frac{Z_4}{2\tau^3}-\frac{Z_3}{2\tau^2}\right)\right)B_{\alpha+1} \tag{30}$$

$$G_{m-1}=\left(\frac{Z_2}{\tau}-\frac{Z_3}{\tau^2}\right)B_\alpha+\left(\left(Z_1-\frac{Z_2}{\tau}\right)-\left(\frac{Z_2}{\tau}-\frac{Z_3}{\tau^2}\right)\right)B_{\alpha+1} \tag{31}$$

$$G_m=\left(\frac{Z_3}{\tau^2}\right)B_\alpha+\left(\left(\frac{Z_2}{\tau}\right)-\left(\frac{Z_3}{\tau^2}\right)\right)B_{\alpha+1} \tag{32}$$

The matrices Z_1-Z_4 in $(29)-(32)$ are presented and expressed explicitly in terms of matrices Z_0 and A^{-1} as follow

$$\mathbf{Z_0}=e^{A\tau} \tag{33}$$

$$\mathbf{Z_1}=\int_0^\tau e^{A\varepsilon}\,d\varepsilon=A^{-1}(e^{A\tau}-I)=A^{-1}(\mathbf{Z_0}-\mathbf{I}) \tag{34}$$

$$\mathbf{Z_2}=\int_0^\tau \varepsilon e^{A\varepsilon}\,d\varepsilon=\varepsilon A^{-1}e^{A\tau}-A^{-1}\int_0^\tau e^{A\varepsilon}\,d\varepsilon=A^{-1}(\mathbf{Z_0}-\tau^{-1}\mathbf{Z_1}) \tag{35}$$

$$\mathbf{Z_3}=\int_0^\tau \varepsilon^2 e^{A\varepsilon}\,d\varepsilon=A^{-1}(\mathbf{Z_0}-2\tau^{-2}\mathbf{Z_2}) \tag{36}$$

$$\mathbf{Z_4}=\int_0^\tau \varepsilon^3 e^{A\varepsilon}\,d\varepsilon=A^{-1}(\mathbf{Z_0}-3\tau^{-3}\mathbf{Z_3}) \tag{37}$$

DOI : 10.31695/IJERAT.2021.3721

Equation (27) can also be expressed as follows :

$$\boldsymbol{u}_{\alpha+1} = [I - \mathbf{G}_{\boldsymbol{\alpha+1}}]^{-1}[\mathbf{G}_{\boldsymbol{\alpha}}\mathbf{u}_{\alpha} + \mathbf{G}_{\boldsymbol{\alpha-1}}\mathbf{u}_{\alpha-1} - \mathbf{G}_{\mathbf{m-1}}\mathbf{u}_{\alpha+1-m} - \mathbf{G}_{\mathbf{m}}\mathbf{u}_{\alpha-m}] \tag{38}$$

If $[I - G_{\alpha+1}]^{-1}$ exists then the matrix form of (38) is as follows

$$\begin{Bmatrix} \mathbf{u}_{\alpha+1} \\ \mathbf{u}_{\alpha} \\ \mathbf{u}_{\alpha-1} \\ \vdots \\ \mathbf{u}_{\alpha+3-k} \\ \mathbf{u}_{\alpha+2-k} \\ \mathbf{u}_{\alpha+1-m} \end{Bmatrix} = \begin{bmatrix} \mathbf{S}^{1,1} & \mathbf{S}^{1,2} & 0 & \cdots & 0 & \mathbf{S}^{1,m} & \mathbf{S}^{1,m+1} \\ \mathrm{I} & 0 & 0 & \cdots & 0 & 0 & 0 \\ 0 & \mathrm{I} & 0 & \cdots & 0 & 0 & 0 \\ 0 & 0 & \vdots & \ddots & \vdots & \vdots & \vdots \\ 0 & 0 & 0 & \cdots & 0 & 0 & 0 \\ 0 & 0 & 0 & \cdots & \mathrm{I} & 0 & 0 \\ 0 & 0 & 0 & \cdots & 0 & \mathrm{I} & 0 \end{bmatrix} \begin{Bmatrix} \mathbf{u}_{\alpha} \\ \mathbf{u}_{\alpha-1} \\ \mathbf{u}_{\alpha-2} \\ \vdots \\ \mathbf{u}_{\alpha+2-k} \\ \mathbf{u}_{\alpha+1-k} \\ \mathbf{u}_{\alpha-m} \end{Bmatrix} \tag{39}$$

Where

$$\mathbf{S}^{1,1} = [I - \mathbf{G}_{\alpha+1}]^{-1}G_{\alpha} \tag{40}$$

$$\mathbf{S}^{1,2} = [I - \mathbf{G}_{\alpha+1}]^{-1}G_{\alpha} \tag{41}$$

$$\mathbf{S}^{1,\mathrm{m}} = [I - \mathbf{G}_{\alpha+1}]^{-1}G_{m-1} \tag{42}$$

$$\mathbf{S}^{1,\mathrm{m+1}} = [I - \mathbf{G}_{\alpha+1}]^{-1}G_{m} \tag{43}$$

According to (39), the discrete map can be expressed as

$$\boldsymbol{u}_{\alpha} = \boldsymbol{D}_{\alpha-1}\boldsymbol{u}_{\alpha-1} = \boldsymbol{D}_{\alpha-1}\boldsymbol{D}_{\alpha-2}\boldsymbol{u}_{\alpha-2} = \cdots = \boldsymbol{D}_{\alpha-1}\boldsymbol{D}_{\alpha-2}\boldsymbol{D}_{\alpha-3}\ldots\boldsymbol{D}_{0}\boldsymbol{u}_{0} \tag{44}$$

The transition matrix Ψ is given by the simple matrix multiplication. It gives the connection between $\boldsymbol{y}_0$ and $\boldsymbol{y}_{\alpha}$ in the form below

$$\Psi = \boldsymbol{D}_{\alpha-1}\boldsymbol{D}_{\alpha-2}\boldsymbol{D}_{\alpha-3}\ldots\boldsymbol{D}_{0} \tag{45}$$

3 APPLICATION OF NUMERICAL SIMULATION OF THE MILLING STABILITY

General description of (1) is required for numerical simulation which is different from SDOF to two DOF.

3.1 Single degree of freedom

The dynamic of a single degree of freedom taking regenerative effect in to consideration (SDOF) milling model can be presented according to [19,30, 31] as follow:

$$m_t\ddot{u}(t) + 2m_t\varepsilon\omega_n\dot{u}(t) + m_t\omega_n^2u(t) = wh_u(t)\big(u(t-T) - u(t)\big) \tag{46}$$

Where $u(t)$, is the position of the tool edge at the time instant t $\omega_n = \sqrt{k/m_t}$ is the angular natural frequency, $\varepsilon = c/(2m_t\omega_n)$ is the relative damping, w is the deph of cut, m_t is the modal mass, $u(t-T)$ is the delay term owing to regenerative result and $h_u(t)$ is dynamic instantaneous uncut chip thickness and presented like that

$$h_u(t) = \sum_{j=1}^{N} g\left(\theta_j(t)\right)\sin\left(\theta_j(t)\right)\left[K_t\cos\left(\theta_j(t)\right) + K_n\sin\left(\theta_j(t)\right)\right] \tag{47}$$

K_t and K_n are the tangential and the normal linearised cutting force coefficients, respectively, and $\theta_j(t)$ is the angular position of the jth tooth

$$\theta_j(t) = \left(\frac{2\pi\Omega}{60}\right)t + \frac{(j-1)2\pi}{N} \tag{48}$$

The function $g(\theta_j(t))$ is a screen function it is equal to 1 if the cutter j is in the cut, and it is equal to 0, if tooth j is out of cut:

DOI : 10.31695/IJERAT.2021.3721

$$g(\emptyset_j(t)) = \begin{cases} 1 \ if \ \theta_s \le \theta_j(t) \le \phi_e \\ 0 \ otherwise \end{cases} \quad (49)$$

Were θ_s and θ_e are respectively the start and exit angles of the jth cutter tooth defined as:

- For down-milling $\theta_{st} = arcos(2a - D)/D$, $\theta_{ex} = \pi$;
- for Up-milling $\theta_{st} = 0$, $\theta_{ex} = arcos(D - 2a)/D$.
- . a/D is the radial immersion ratio, a is the radial deph of cut and D is the diameter of the cutter.

The matrices and the state vector of (1) according to the single degree of freedom are represented as follow :

$$\mathbf{A} = \begin{bmatrix} -\varepsilon\omega_n & \frac{1}{m_t} \\ m_t(\varepsilon\omega_n)^2 & -\varepsilon\omega_n \end{bmatrix}, \mathbf{B}(t) = \begin{bmatrix} 0 & 0 \\ -h_u(t) & 0 \end{bmatrix}, \mathbf{C}(t) = \begin{bmatrix} 0 & 0 \\ h_u(t) & 0 \end{bmatrix} \text{and } \mathbf{u}(t) = \{\mathrm{u}(t) \quad \dot{\mathrm{u}}(t)\}^T$$

3.2 Two degree of freedom

The dynamic equation of a two degree of freedom milling model taking regenerative effect into consideration with a symmetric tool is presented as follow according to

$$\begin{bmatrix} m_{tu} & 0 \\ 0 & m_{tv} \end{bmatrix}\begin{bmatrix} \ddot{u}(t) \\ \ddot{v}(t) \end{bmatrix} + \begin{bmatrix} 2\varepsilon\omega_{nu} & 0 \\ 0 & 2\varepsilon\omega_{nv} \end{bmatrix}\begin{bmatrix} \dot{u}(t) \\ \dot{v}(t) \end{bmatrix} + \begin{bmatrix} m_{tu}\omega_{nu}^2 & 0 \\ 0 & m_t\omega_{nv}^2 \end{bmatrix}\begin{bmatrix} u(t) \\ v(t) \end{bmatrix} = \begin{bmatrix} -wh_{uu}(t) & -wh_{uv}(t) \\ -wh_{vu}(t) & -wh_{vv}(t) \end{bmatrix}\begin{bmatrix} u(t) \\ v(t) \end{bmatrix} + \begin{bmatrix} wh_{uu}(t) & wh_{uv}(t) \\ wh_{vu}(t) & wh_{vv}(t) \end{bmatrix}\begin{bmatrix} u(t-T) \\ v(t-T) \end{bmatrix} \quad (50)$$

Where $u(t)$ is the position of the tool edge at the time instant t, $\omega_{nu} = \sqrt{k_u/m_{tu}}$ $\omega_{nv} = \sqrt{k_v/m_{tv}}$ is the angular natural frequency, $\varepsilon_u = \sqrt{k_u/m_{tu}} = c_u/(2m_{tu}\omega_{nu})$, $\varepsilon_v = \sqrt{k_v/m_{tv}} = c_v/(2m_{tv}\omega_{nv})$ is the relative damping, w is the deph of cut, m_{tu}, m_{tv} is the modal mass, $h_{uu}(t)$, $h_{vv}(t)$, $h_{vu}(t)$, $h_{uv}(t)$ are the cutting force coefficients defined as follow:

$$h_{uu}(t) = \sum_{j=1}^{N} g\left(\theta_j(t)\right)\sin\left(\theta_j(t)\right)\left[K_t\cos\left(\theta_j(t)\right) + K_n\sin\left(\theta_j(t)\right)\right] \quad (51)$$

$$h_{uv}(t) = \sum_{j=1}^{N} g\left(\theta_j(t)\right)\cos\left(\theta_j(t)\right)\left[K_t\cos\left(\theta_j(t)\right) + K_n\sin\left(\theta_j(t)\right)\right] \quad (52)$$

$$h_{vu}(t) = \sum_{j=1}^{N} g\left(\theta_j(t)\right)\sin\left(\theta_j(t)\right)\left[-K_t\sin\left(\theta_j(t)\right) + K_n\cos\left(\theta_j(t)\right)\right] \quad (53)$$

$$h_{vv}(t) = \sum_{j=1}^{N} g\left(\theta_j(t)\right)\cos\left(\theta_j(t)\right)\left[-K_t\sin\left(\theta_j(t)\right) + K_n\cos\left(\theta_j(t)\right)\right] \quad (54)$$

The matrices and the state vector of (1) according to the two DOF are presented as follow :

$$\mathbf{A(t)} = \begin{bmatrix} 0 & 0 & 1 & 0 \\ 0 & 0 & 0 & 1 \\ -\omega_n^2 & \mathbf{0} & -2\varepsilon\omega_{nu} & 0 \\ \mathbf{0} & -\omega_n^2 & 0 & -2\varepsilon\omega_{nv} \end{bmatrix} \quad (55)$$

$$\mathbf{B(t)} = \begin{bmatrix} 0 & 0 & 0 & 0 \\ 0 & 0 & 0 & 0 \\ -\frac{wh_{xx}(t)}{m_t} & -\frac{wh_{xy}(t)}{m_t} & 0 & 0 \\ -\frac{wh_{vu}(t)}{m_t} & -\frac{wh_{vv}(t)}{m_t} & 0 & 0 \end{bmatrix} \quad (56)$$

DOI : 10.31695/IJERAT.2021.3721

$$\mathbf{C(t)} = \begin{bmatrix} 0 & 0 & 0 & 0 \\ 0 & 0 & 0 & 0 \\ \frac{wh_{uu}(t)}{m_t} & \frac{wh_{uv}(t)}{m_t} & 0 & 0 \\ \frac{wh_{vu}(t)}{m_{tu}} & \frac{wh_{vv}(t)}{m_{tv}} & 0 & 0 \end{bmatrix} \quad (57)$$

4 STABILITY LOBES DIAGRAMS

In this study the domain of cutting parameter for mapping stability lobes diagram is set as: the spindle speed ranges from 5000 rpm to 25000rpm, and the depth of cut w ranges from 0 to 10mm. The reference red line is computed by the first order full discretization method with m=500. The radial immersion ratio per cent a/D set as 100%, 75%, 50%, 25%, 10%, 5% respectively for down- milling and up- milling. The stability demoted by the green line is compute by the second order full-discretization with m=23 and over 200×100 sized grid of parameters. The dynamics parameters are shown in the **table 1**. The parameters used in all numerical computations in this work which are identical with the experimentally determined parameters of [33] are compiled in Table 1. Table 1 reflects symmetry of the 2DOF tool for which parameters are the same in the feed and feed normal directions. The properties of the laptop computer used for computations are as follows: Processor: intel(R) Celeron(R) CPU1005M@ 1.90GHz 1.90GHz; Installed Memory (RAM): 4.00 GB (3..88GHz usable); System type: 64-bit operating system.

Table 1: Dynamics parameters for numerical computational of stability lobes diagrams.

$\boldsymbol{\omega_n}$	$\boldsymbol{4793rad/s}$
$\boldsymbol{\varepsilon}$	0.011
$\mathbf{K_t}$	$6 \times 10^8 \mathrm{N/m^2}$
$\mathbf{K_n}$	$2 \times 10^8 \mathrm{N/m^2}$
$\mathbf{m_t}$	0.03993 kg
N	2
$\boldsymbol{\omega_{nu} = \omega_{nv}}$	$4793rad/s$
$\boldsymbol{\varepsilon_u = \varepsilon_v}$	0.011
$\boldsymbol{m_{tu} = m_{tv}}$	$0.03993\ kg$

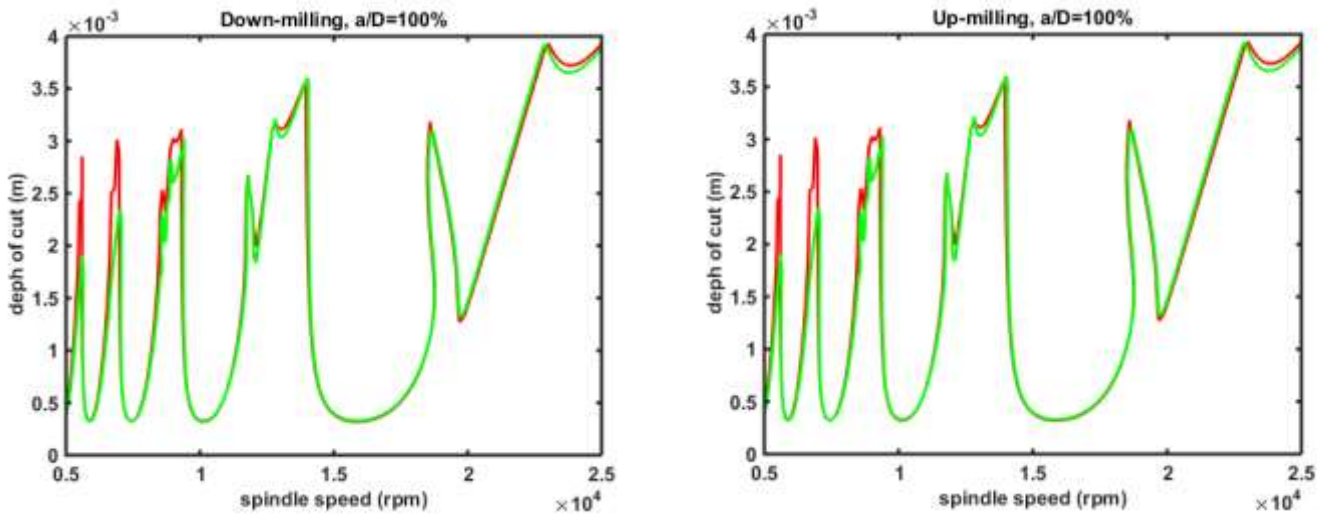

Figure.1 stability lobes diagrams up-milling and down-milling SDOF model predicted by the 2nd FDM for full immersion ratio per cent (a/D=100%),

DOI : 10.31695/IJERAT.2021.3721

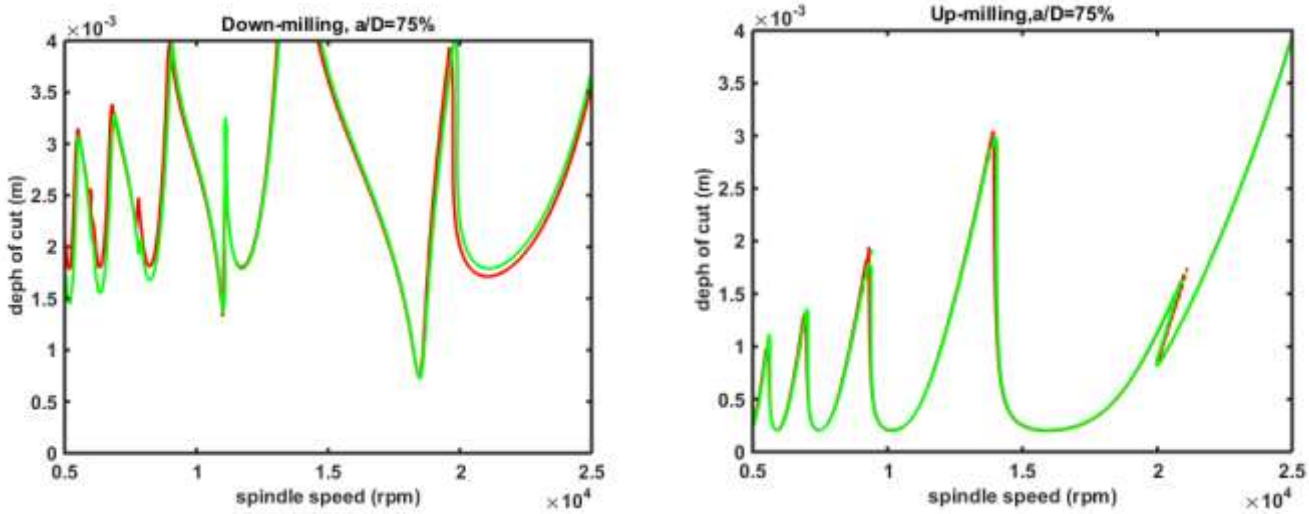

Figure.2 stability lobes diagrams up-milling and down-milling SDOF model predicted by the 2nd FDM for full immersion ratio per cent (a/D=75%),

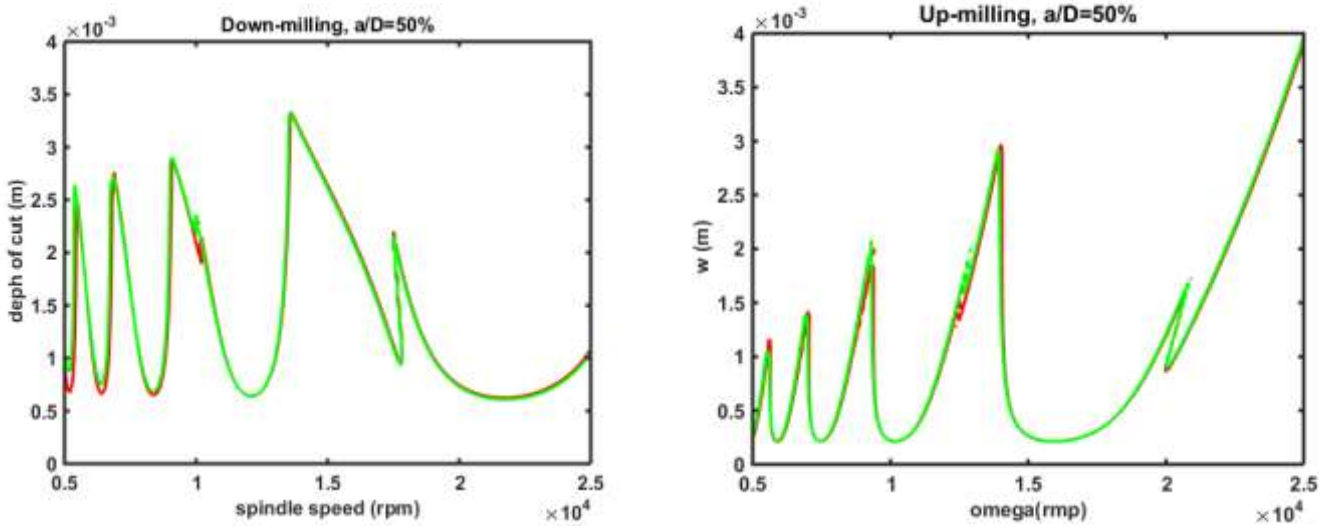

Figure.3 stability lobes diagrams up-milling and down-milling SDOF model predicted by the 2 nd FDM for full immersion ratio per cent (a/D=50%)

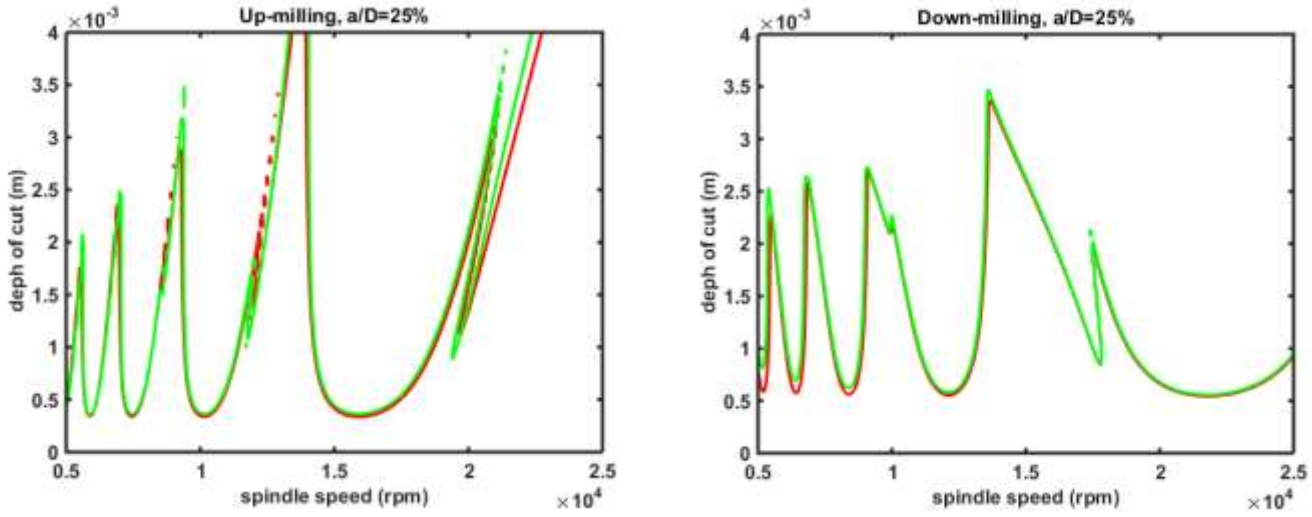

Figure.4 stability lobes diagrams up-milling and down-milling SDOF model predicted by the 2nd FDM for full immersion ratio per cent (a/D=25%),

DOI : 10.31695/IJERAT.2021.3721

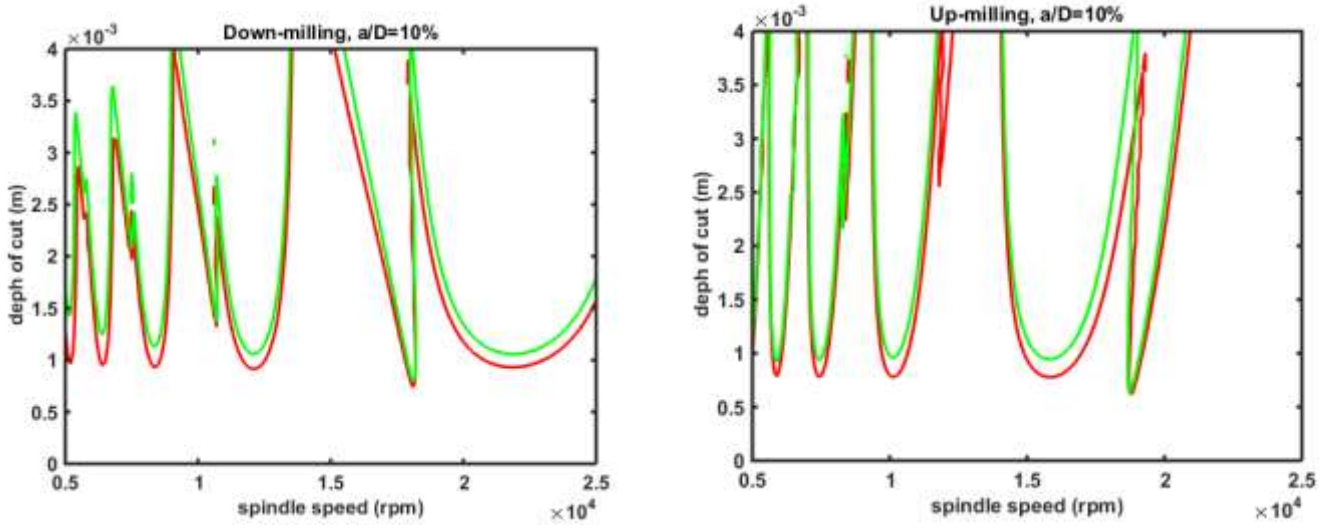

Figure.5 stability lobes diagrams up-milling and down-milling SDOF model predicted by the 2 nd FDM for full immersion ratio per cent (a/D=10%)

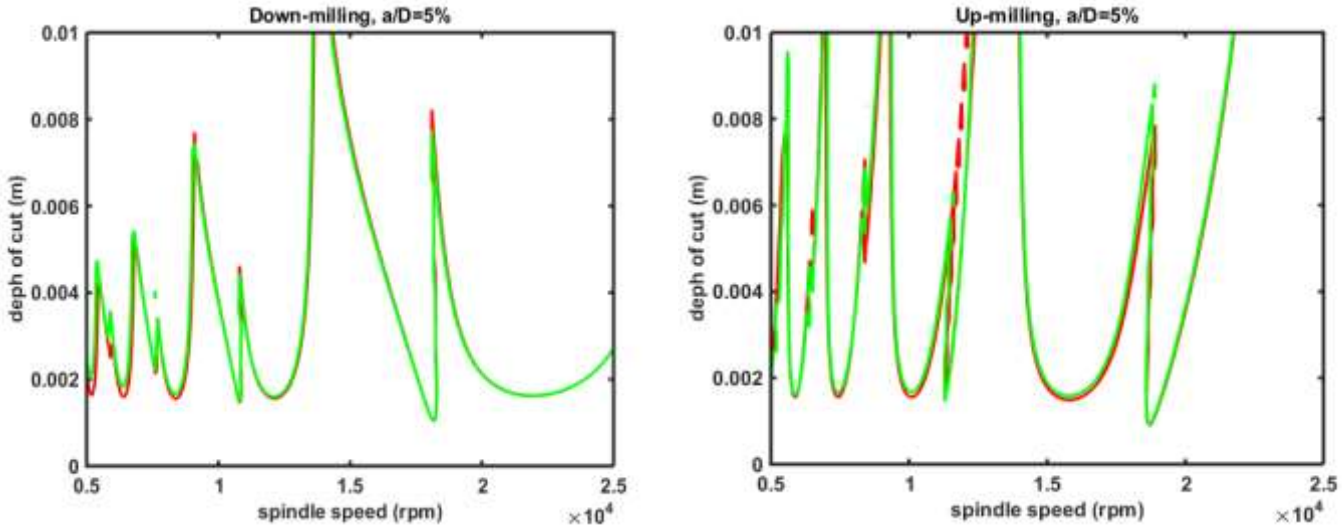

Figure.6 stability lobes diagrams up-milling and down-milling SDOF model predicted by the 2nd FDM for full immersion ratio per cent very low immersion(a/D=5%)

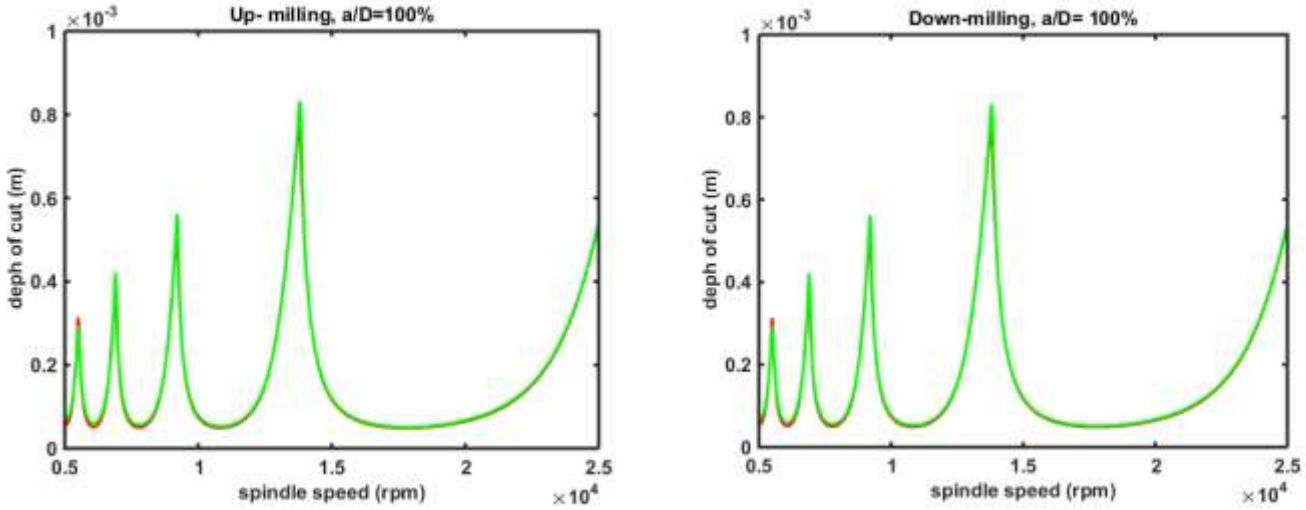

Figure.7: A Stability lobes diagrams up-milling and down-milling 2DOF model predicted by the 2nd FDM for full immersion ratio per cent (a/D=100%)

DOI : 10.31695/IJERAT.2021.3721

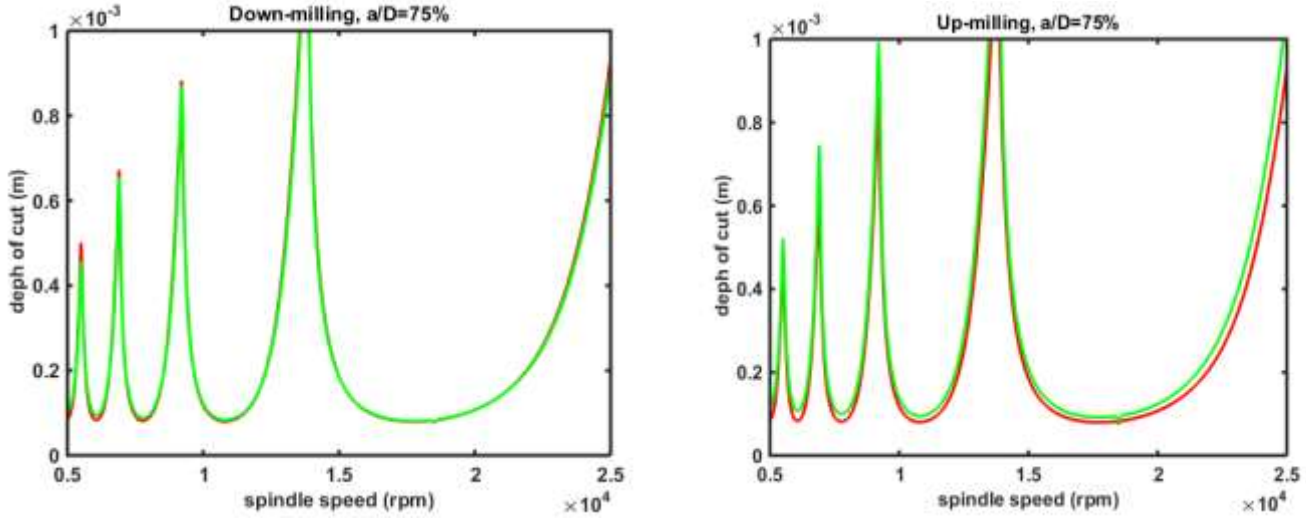

Figure.8: A Stability lobes diagrams up-milling and down-milling 2DOF model predicted by the 2nd FDM three quarter immersion (a/D=75%),

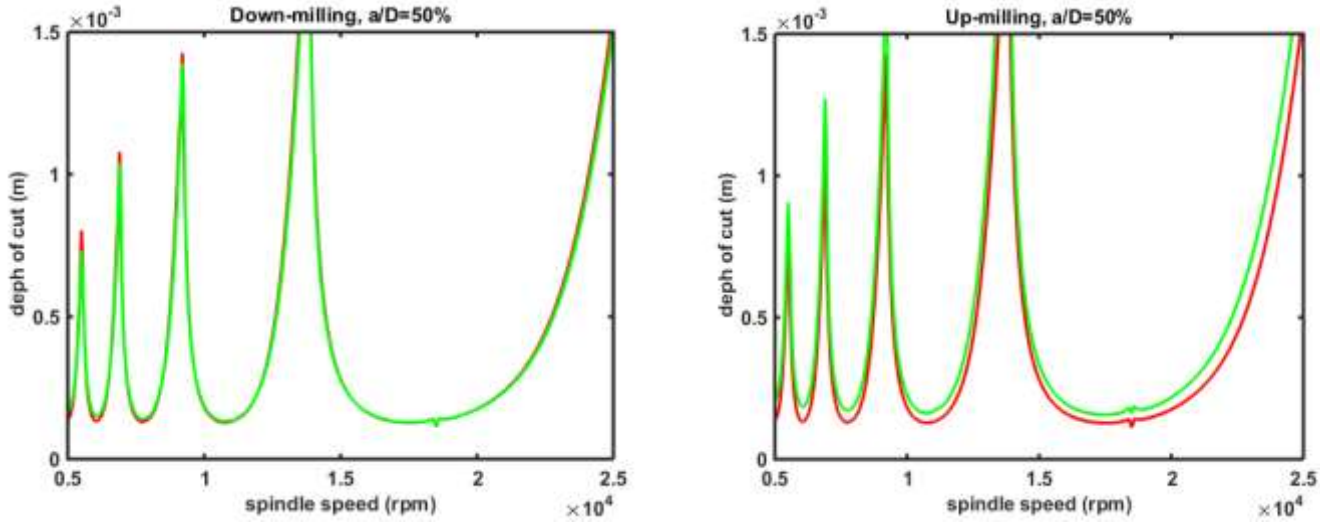

Figure.9: A Stability lobes diagrams up-milling and down-milling 2DOF model predicted by the 2nd FDM for half immersion (a/D=50%)

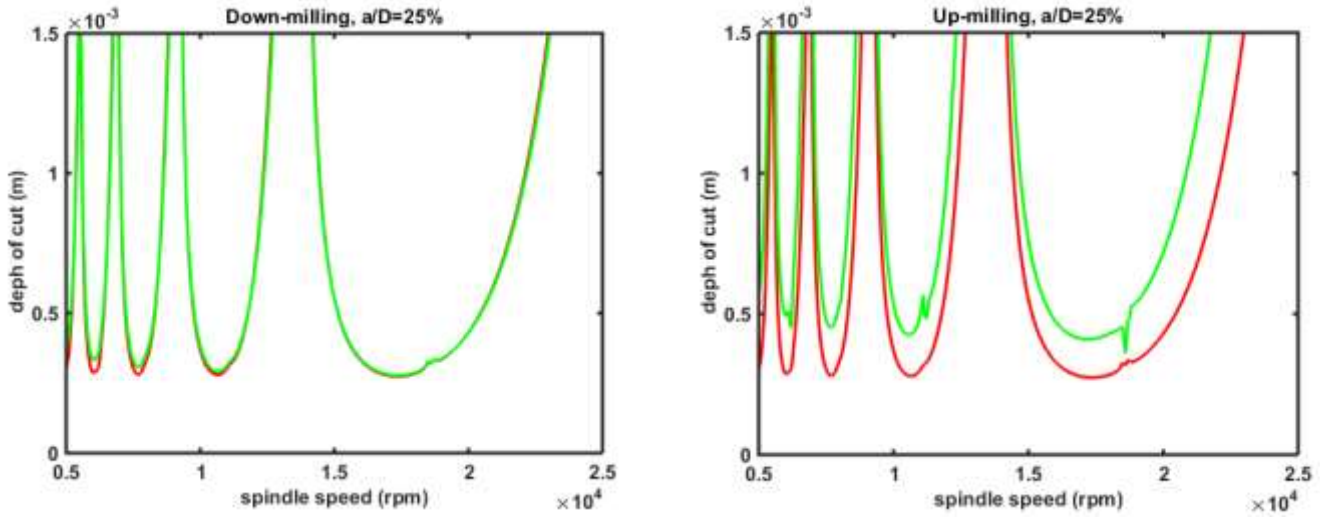

Figure.10: A Stability lobes diagrams up-milling and down-milling 2DOF model predicted by the 2nd FDM for low immersion (a/D=10%)

DOI : 10.31695/IJERAT.2021.3721

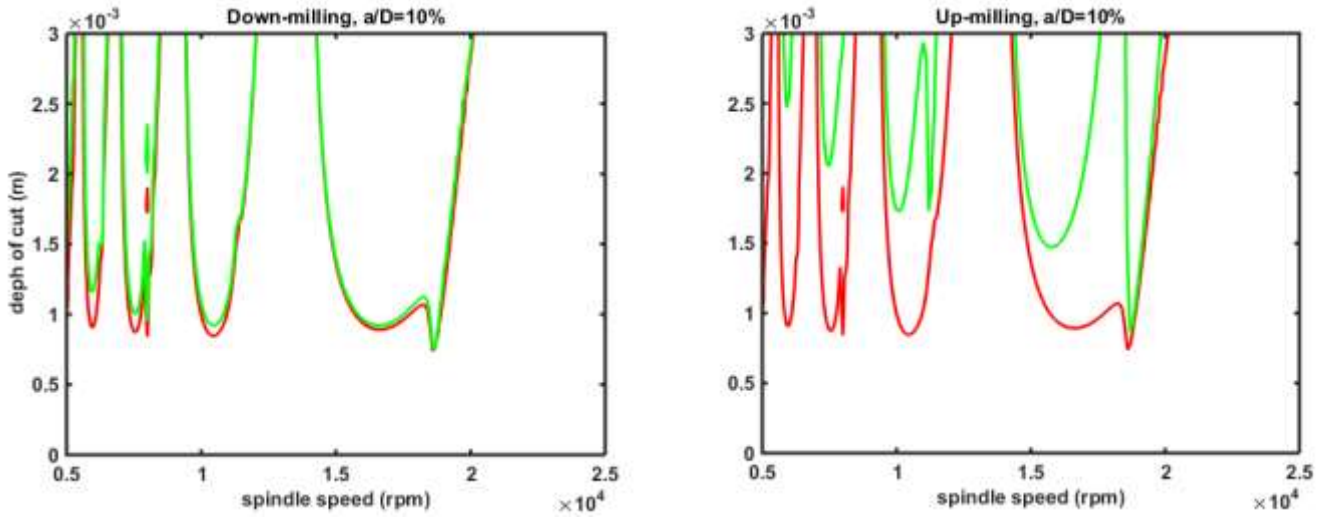

Figure.11: A Stability lobes diagrams up-milling and down-milling 2DOF model predicted by the 2nd FDM for low immersion (a/D=10%)

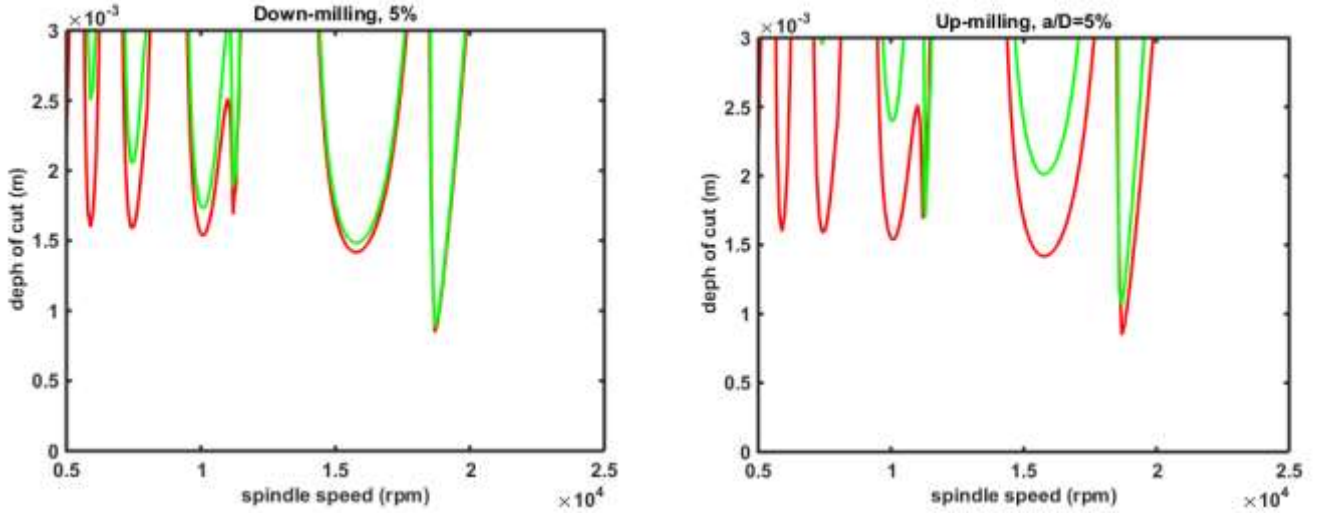

Figure.12: A Stability lobes diagrams up-milling and down-milling 2DOF model predicted by the 2nd FDM for very low immersion (a/D=5%)

The stability lobes diagrams presentd in **figures 1** to **12** show that in the general case the immersion ratio is a factor that greatly influences the plot of the stability diagram . The curves themselves is the boundary area between the stable domain below the curve, i.e. the area where the machining is vibration-free. It corresponds to the zone where the possible torques between the speed of rotation of the cutter and the equivalent depth of cut will be chosen without risk of vibration leading to the regenerative effect and the unstable zone above the curve, that is to say the risk zone or the choice of the speed of rotation and the depth of cut must be avoided, as there is a risk of vibration leading to the very delicate phenomenon without return that the machiner will encounter called chatter.

DOI : 10.31695/IJERAT.2021.3721

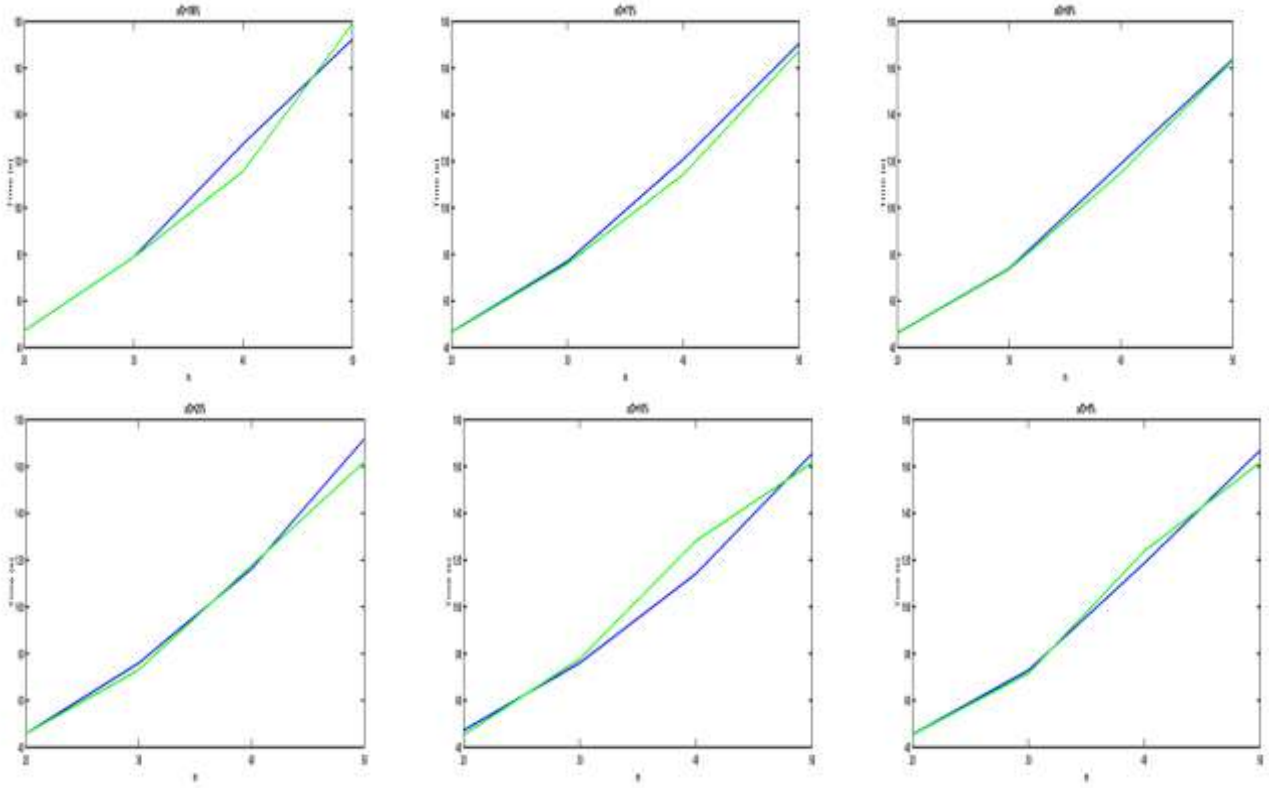

Figure 13. Influence of the calculation parameter on the calculation time of the eigenvalues for the SDOF case for up milling (green) and down-milling (blue)

It is seen from **figure 1** that for full immersion the stability lobe diagrams obtained for down-milling operation is almost identical to that obtained by up-milling for both one degree and two degree of freedom. In general cases the stability lobes diagrams for down- milling are much closer to the ideal curves than up- milling for the differnts values of radial immersion ratio. For three-quarter immersion, down-milling has a wider zone of general stability than for up- milling. From 5000rpm to 20,000rpm, the stability zone is much greater in down-milling than in up-milling. Beyond 20,000rpm the latter will be more profitable. This means that for materials so the high speed rotational or spindle speed range above 20,000rpm, up-milling will be more efficient. The similar case is observed for the case of half-immersion. The horizontal stability limit has changed from 1mm at 75% to 0.75mm at 50%. The peak of stability is higher in milling while swallowing for the quarter immersion. The horizontal stability limit is greater than 0.5mm in down-milling is less than 0.5mm in up-milling. In the case of quarter immersion for a spindle speed greater than 20,000rpm, up-milling will be more efficient than down-milling. For low and very low immersion the stability limit is almost equal for up- and down- milling. For values greater than 20,000rpm, the preference is for the up-milling side while swallowing given the range of depth of cut that it offers us. Milling is possible for a depth of cut up to a value greater than 4mm for up- milling hence its need for cutting speeds greater than 20,000rpm.

In case of 2DOF, for full immersion ratio **figure 7**, the stability lobe diagrams obtained for down-milling operation is too identical to that obtained by up-milling for two degree of freedom and the stability lobe diagrams for down- milling are much closer to the ideal curves than up- milling too for the differents values of radial immersion ratio. For three quarter immersion ratio (**figure 8**), down- milling is much accuracy than up-milling with the same stability domain and the same horizontal stability limit. The pic of stability is approximatively the same but the domain of stability of down-milling is larger than up-milling domain. Although half immersion ratio **figure 9** presented the same limit of stability horizontal for the two cases and down- milling accuracy than up-milling the stability domain is approximatively the same. For quarter immersion ratio **figure 10**, down milling in accuracy than up-milling although they have same limit of stability.For low immersion ratio **figure 11**, and very low immersion ratio **figure 12,** the accuracy of down-milling is better than up milling. The observation in the general case is that the up-milling is less accuracy than the down milling for the different values of the immersion ratio except the case of the total immersion. **Figure 13** shows how the calculation parameter has impact to the calculation time for both up and down milling. Green represents up-milling and blue is for down-milling. When the calculation parameter $m < 30$ the calculation time is practically equal for the differents values of a/D. For a/D=100% up- milling is better efficient than down- milling when $30 < m < 45$. The opposite is observed for a/D=10% ie up-milling is less efficient than down-milling. For three quarter immersion ratio per cent, down milling is better efficient than up milling when $m > 30$. For half immersion, quarter immersion and very low immersion the difference is not enough.

DOI : 10.31695/IJERAT.2021.3721

5 RATE OF CONVERGENCE FOR SDOF

The convergence rate describes the calculation accuracy of numerical methods i.e. how fast the approximate solution converges to the exact one. **In Figure 14** and **figure 15** the term $\big||\boldsymbol{\beta}| - |\boldsymbol{\beta_0}|\big|$ is called the convergence rates. It reflects the local errors between the absolute value of the maximal critical eigenvalues of the state transition matrix $|\boldsymbol{\beta}|$, function of computational parameter and the exact one $|\boldsymbol{\beta_0}|$**.** the convergence rates of SDM, 1st FDM and 2nd FDM is presented in **figure 14** and **figure 15**. The radial immersion ratio a/D is set as 45% and 10% and for speendle speed $\Omega = 10000\text{rpm}$ and $\Omega = 7500\text{rpm}$ speed respectively. the convergence of the critical eigenvalues $|\boldsymbol{\beta}|$, are calculated using various methods with respect to different discretization intervals m over one tooth passing period. For reference, is determined by the 1stFDM with M=1250.

The cutting parameters for rate of convergence in **Figure 14** are: $\Omega = 7500\text{rpm}$, $\text{w} = 1.1\text{mm}$, $\text{w} = 2\text{ mm}$ and $\text{w} = 2.9\text{mm}$. In general cases the computational precision of SDM is the lowest when $m \leq 100$. As shown in **figure 14a**. 2nd FDM has the higher rate of convergence than 1st FDM and SDM. The computational precision of SDM is the lowest when m <100, though its local discretization error is less than that of 1st FDM and 2ndFDM. As shown in **figure 14.b** the computational precision of 2ndFDM is higher than the two method when $m \leq 30$. For $m \geq 85$ the rate of convergence is the same for 1st FDM and 2ndFDM. Though its local discretization error is more than that of SDM**.** In **figure 14c**. 1st FDM has the higher rate of convergence than SDM and 2nd FDM.

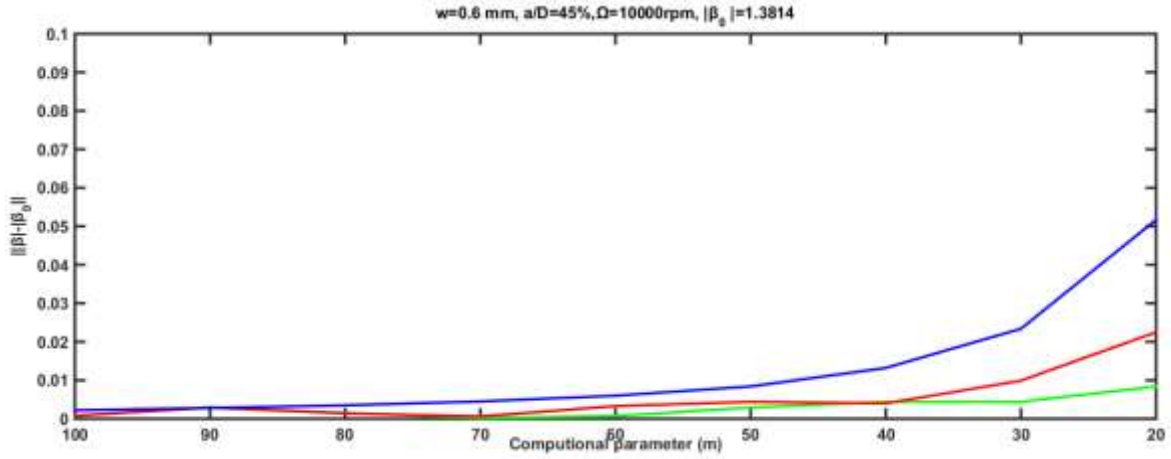

(a) **Convergence rates of the semi-discretization method (blue color) , first order full-discretization method (green color), and second order full-discretization method (red color) with axial death of cut** $w = 0.6mm$

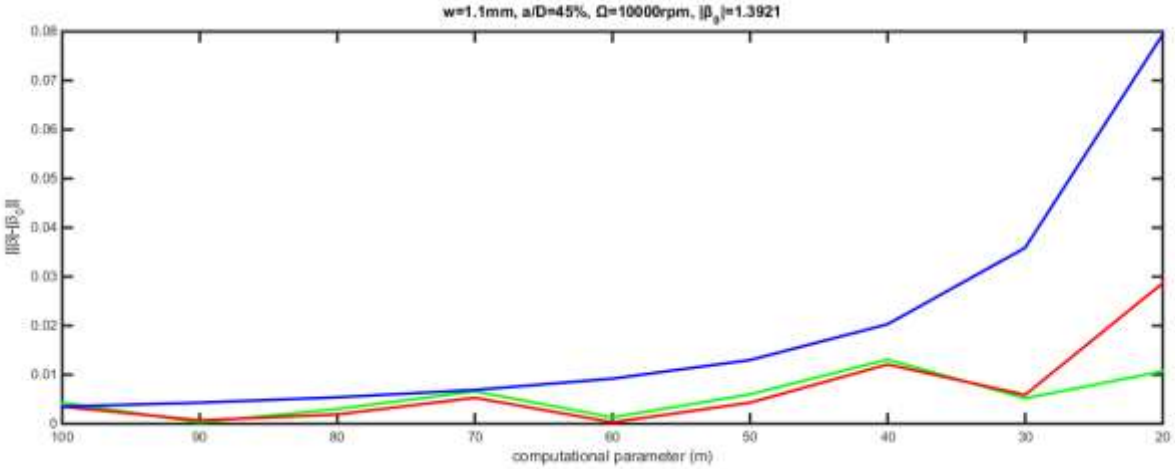

(b) Convergence rates of the semi-discretization method (blue color) , first order full-discretization method (red color), and second order full-discretization method (green color) with axial death of cut $w = 1.1mm$

.

DOI : 10.31695/IJERAT.2021.3721

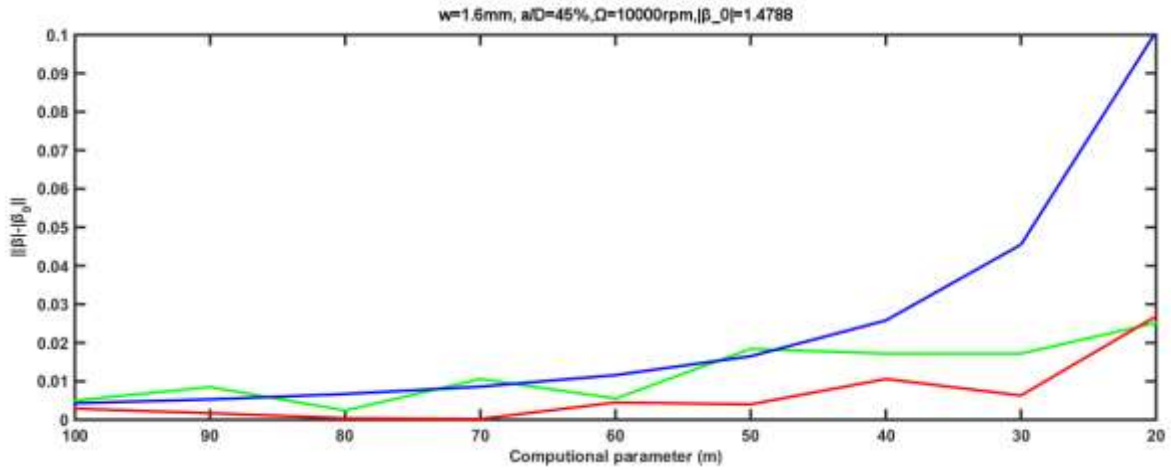

(c) Convergence rates of the semi-discretization method (blue color) , first order full-discretization method (red color), and second order full-discretization method (green color) with axial death of cut $w = 1.6mm$

Figure 14. Convergence rates of the SDM, 1st FDM, and 2nd FDM the proposed method with the radial immersion ratio a/D=45%)

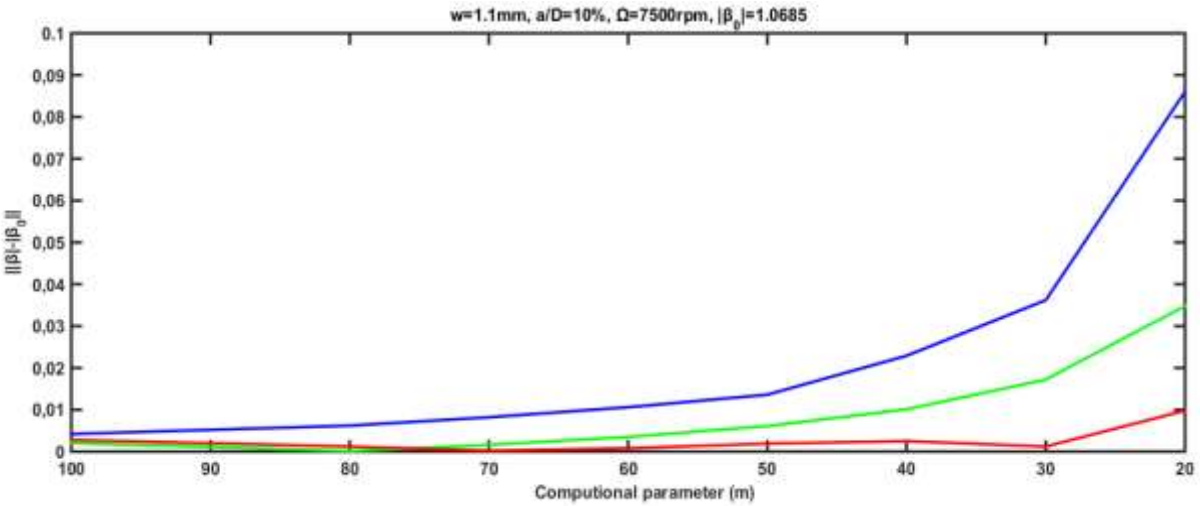

(a) Convergence rates of the semi-discretization method (blue color) , first order full-discretization method (red color), and second order full-discretization method (green color) with axial death of cut $w = 1.1mm$

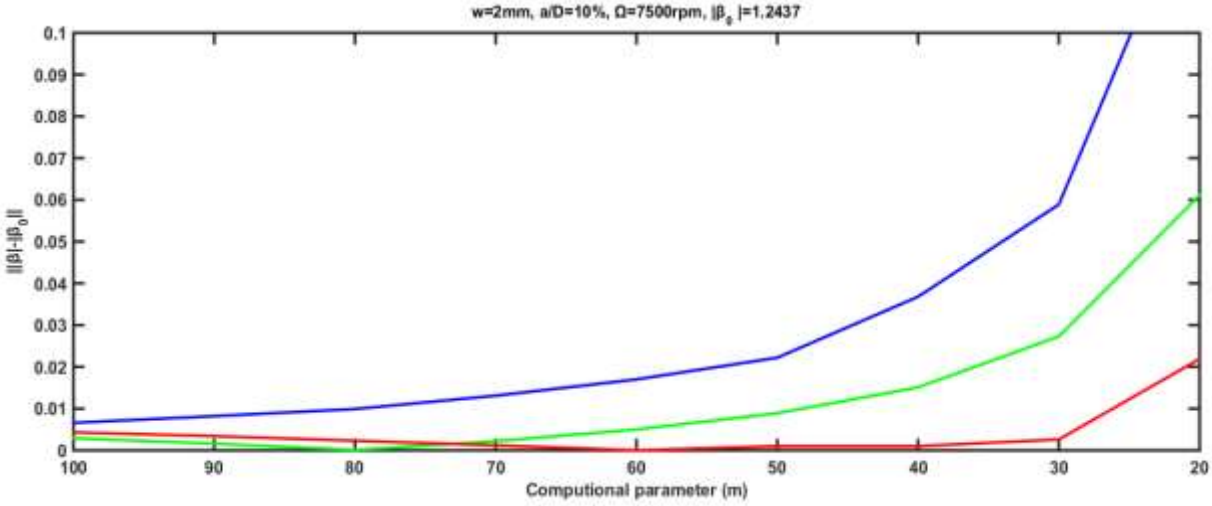

(b) Convergence rates of the semi-discretization method (blue color) , first order full-discretization method (red color), and second order full-discretization method (green color) with axial death of cut $w = 2mm$

DOI : 10.31695/IJERAT.2021.3721

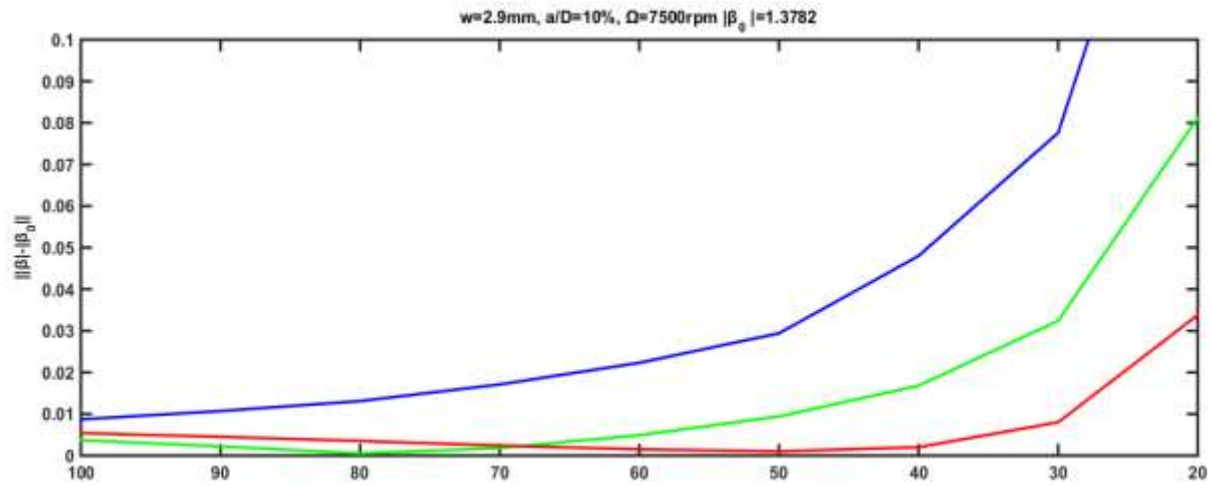

(c) Convergence rates of the semi-discretization method (blue color), first order full-discretization method (red color), and second order full-discretization method (green color) with axial death of cut $w = 2.9mm$

Figure 15. Convergence rates of the SDM, 1st FDM**,** and 2ndFDM **the proposed method with the radial immersion ratio a/D=10%)**

In the second case **figure 15** the rate of convergence is for a low radial immersion ratio, The cutting parameters use for the case are: $\Omega = 10000\text{rpm}$, $w = 0.6\text{mm}$, $w = 1.6\text{mm}$ and $w = 2.9\text{mm}$. The 2ndFDM has the best computational precision is higher than the two methods when a/D=10%, $\Omega = 10000\text{rpm}$, $w = 0.6\text{mm}$ and $m \geq 75$. In the other way 1st FDM has the best rate of convergence. It is shown in **figure 15c** that the rate of convergence of 2ndFDM is higher than the two others method. 2FDM is reliable and accurate for stability prediction only when the approximation parameter m is larger enough (m≥70), while $m < 70$ 1stFDM have more . The computational precision of SDM is the lowest when $m < 100$.

6 CONCLUSION

A higher order semi-analytical method so-called second order full discretisation method is applyed in solving the chatter stability problem for up and down-milling. It is found in this work that the stability chart of SDOF case is generally seen to be had much greater stable sub-space than the corresponding 2DOF case. And the radial immersion is a factor that greatly influences the plot of the stability lobes diagram. The increase of parameter m leads to increase of time varying. For full immersion up and down milling stability lobes are identical but there is little different of computational time, down-milling is efficient. The comparison of up and down-milling in case of SDOF based from observation from 5000rpm to 20,000rpm, the stability zone is much greater in down-milling than in up-milling. Beyond 20,000rpm the latter will be more profitable. This means that for materials so the high speed rotational or spindle speed range above 20,000rpm, up-milling will be more efficient. In general cases of 2DOF a part from full immersion which present the same stability lobe diagram for both up- and down-milling, down-milling present better diagram of stability than up-milling in term of advantages and accuracy. And the increase in the stability zone is caused by the decrease in the immersion ratio. Down milling has computational efficiency than up-milling for both SDOF and 2DOF. In term of accuracy in about all cases down-milling is better than up-milling. 2ndFDM has better accuracy for very high calculation parameter.

REFERENCES

1. Tobias, S. A., & Fishwick, W. (1958). Theory of regenerative machine tool chatter. *The engineer*, *205*(7), 199-203.
2. Tlusty, J. (1963). The stability of the machine tool against self-excited vibration in machining. *Proc. Int. Res. In Production Engineering, Pittsburgh, ASME*, *465*.
3. Zhang, X. J., Xiong, C. H., Ding, Y., Feng, M. J., & Xiong, Y. L. (2012). Milling stability analysis with simultaneously considering the structural mode coupling effect and regenerative effect. *International Journal of Machine Tools and Manufacture*, *53*(1), 127-140.
4. Munoa, J., Zatarain, M., Dombóvári, Z., & Yang, Y. (2009, May). Effect of mode interaction on stability of milling processes. In *12th CIRP Conference on Modelling of Machining Operations, San Sebastian, Spain* (pp. 927-933).
5. Tlusty, J., & Ismail, F. (1981). Basic non-linearity in machining chatter. *CIRP Annals*, *30*(1), 299-304.
6. Altintaş, Y., & Budak, E. (1995). Analytical prediction of stability lobes in milling. *CIRP annals*, *44*(1), 357-362.

DOI : 10.31695/IJERAT.2021.3721

7. Budak, E., & Altintas, Y. (1998). Analytical prediction of chatter stability in milling—part I: general formulation.
8. Merdol, S. D., & Altintas, Y. (2004). Multi frequency solution of chatter stability for low immersion milling. *J. Manuf. Sci. Eng.*, *126*(3), 459-466.
9. Merdol, S. D., & Altintas, Y. (2004). Multi frequency solution of chatter stability for low immersion milling. *J. Manuf. Sci. Eng.*, *126*(3), 459-466.
10. Butcher, E. A., Ma, H., Bueler, E., Averina, V., & Szabo, Z. (2004). Stability of linear time-periodic delay-differential equations via Chebyshev polynomials. *International Journal for Numerical Methods in Engineering*, *59*(7), 895-922.
11. Butcher, E. A., Ma, H., Bueler, E., Averina, V., & Szabo, Z. (2004). Stability of linear time-periodic delay-differential equations via Chebyshev polynomials. *International Journal for Numerical Methods in Engineering*, *59*(7), 895-922.
12. Insperger, T., & Stépán, G. (2002). Semi-discretization method for delayed systems. *International Journal for numerical methods in engineering*, 55(5), 503-518.
13. Elbeyli, O., & Sun, J. Q. (2004). On the semi-discretization method for feedback control design of linear systems with time delay. *Journal of Sound and Vibration*, 1(273), 429-440.
14. Insperger, T., Stépán, G., & Turi, J. (2008). On the higher-order semi-discretizations for periodic delayed systems. *Journal of Sound and Vibration*, 313(1-2), 334-341.
15. Insperger, T., & Stépán, G. (2004). Updated semi-discretization method for periodic delay-differential equations with discrete delay. *International journal for numerical methods in engineering*, 61(1), 117-141.
16. Henninger, C., & Eberhard, P. (2008). Improving the computational efficiency and accuracy of the semi-discretization method for periodic delay-differential equations. *European Journal of Mechanics-A/Solids*, 27(6), 975-985.
17. Ahmadi, K., & Ismail, F. (2012). Stability lobes in milling including process damping and utilizing multi-frequency and semi-discretization methods. *International Journal of Machine Tools and Manufacture*, 54, 46-54.
18. Wang, M., Gao, L., & Zheng, Y. (2014). Prediction of regenerative chatter in the high-speed vertical milling of thin-walled workpiece made of titanium alloy. *The International Journal of Advanced Manufacturing Technology*, 72(5-8), 707-716.
19. Ding, Y., Zhu, L., Zhang, X., & Ding, H. (2010). A full-discretization method for prediction of milling stability. *International Journal of Machine Tools and Manufacture*, 50(5), 502-509.
20. Ding, Y., Zhu, L., Zhang, X., & Ding, H. (2010). Second-order full-discretization method for milling stability prediction. *International Journal of Machine Tools and Manufacture*, 50(10), 926-932.
21. Quo, Q., Sun, Y., & Jiang, Y. (2012). On the accurate calculation of milling stability limits using third-order full-discretization method. International Journal of Machine Tools and Manufacture, 62, 61-66.
22. Ozoegwu, C. G., & Omenyi, S. N. (2016). Third-order least squares modelling of milling state term for improved computation of stability boundaries. *Production & Manufacturing Research*, 4(1), 46-64.
23. Ozoegwu, C. G., Omenyi, S. N., & Ofochebe, S. M. (2015). Hyper-third order full-discretization methods in milling stability prediction. *International Journal of Machine Tools and Manufacture*, 92, 1-9.
24. Insperger, T. (2010). Full-discretization and semi-discretization for milling stability prediction: some comments. *International Journal of Machine Tools and Manufacture*, 50(7), 658-662.
25. Insperger, T. (2010). Full-discretization and semi-discretization for milling stability prediction: some comments. *International Journal of Machine Tools and Manufacture*, 50(7), 658-662.
26. Niu, J., Ding, Y., Zhu, L., & Ding, H. (2014). Runge–Kutta methods for a semi-analytical prediction of milling stability. *Nonlinear Dynamics*, 76(1), 289-304.
27. Qin, C., Tao, J., & Liu, C. (2019). A novel stability prediction method for milling operations using the holistic-interpolation scheme. Proceedings of the Institution of Mechanical Engineers, Part C: *Journal of Mechanical Engineering Science*, 233(13), 4463-4475.
28. Insperger, T., Mann, B. P., Stépán, G., & Bayly, P. V. (2003). Stability of up-milling and down-milling, part 1: alternative analytical methods. *International journal of Machine tools and manufacture*, 43(1), 25-34.
29. Mann, B. P., Insperger, T., Bayly, P. V., & Stépán, G. (2003). Stability of up-milling and down-milling, part 2: experimental verification. International Journal of Machine Tools and Manufacture, 43(1), 35-40.
30. Insperger, T., & Stépán, G. (2004). Vibration frequencies in high-speed milling processes or a positive answer to Davies, Pratt, Dutterer and Burns. *J. Manuf. Sci. Eng*., 126(3), 481-487.
31. Insperger, T., & Stépán, G. (2000). Stability of the milling process. *Periodica polytechnica mechanical engineering*, 44(1), 47-57.
32. Ozoegwu, C. G. (2014). Least squares approximated stability boundaries of milling process. *International Journal of Machine Tools and Manufacture*, 79, 24-30.

DOI : 10.31695/IJERAT.2021.3721

33. Bayly, P. V., Mann, B. P., Schmitz, T. L., Peters, D. A., Stepan, G., & Insperger, T. (2002, January). Effects of radial immersion and cutting direction on chatter instability in end-milling. In *ASME International Mechanical Engineering Congress and Exposition* (Vol. 3641, pp. 351-363).

DOI : 10.31695/IJERAT.2021.3721